UDC 629.563.24:624.014.2.042.8]:519.6
Original scientific paper
Received: 11.12.2016.

Nonlinear restoring stiffness of triangular tension leg platforms

Ivo Senjanović, Marko Tomić, Smiljko Rudan, Neven Hadžić

University of Zagreb, Faculty of Mechanical Engineering and Naval Architecture, Ivana Lučića 5, 10000 Zagreb, CROATIA
e-mail: ivo.senjanovic@fsb.hr

SUMMARY

A new stiffness matrix for nonlinear dynamic analysis of triangular TLPs is formulated utilising both the equilibrium of forces and energy balance approach for arbitrary surge, sway and yaw. Static numerical analysis is performed for a triangular TLP, ordinarily used as a benchmark in the relevant literature, by imposing surge force and yaw moment. In order to validate the new stiffness formulation, the obtained results are compared with those determined by an FEM analysis. Some shortcomings of the traditionally used stiffness matrix are pointed out.

KEY WORDS: *triangular tension leg platform, nonlinear stiffness, force equilibrium approach, energy balance approach, FEM.*

1. INTRODUCTION

Cost of the fixed offshore structures grows rapidly with the increased water depth. Therefore, development of the compliant offshore structures is encouraged, due to possible minimisation of their response to the environmental loads by the structural flexibility. A typical offshore compliant structure is a tension leg platform (TLP), used extensively in oil gas industry as a semi-submersible structure attached to the sea bottom by vertical pre-tensioned tendons or tethers, [1]. TLP consists of a pontoon, columns and a deck with production equipment, [2]. Additionally, TLP can be used as a floater to support bridge superstructure, [3], and, more recently, to provide support for offshore wind turbine, [4, 5].

TLP performs nonlinear motion in waves due to nonlinear restoring stiffness and damping, [6]. Amplitudes of horizontal motion are much larger than those of vertical motion, since the former and latter depend on low tendon geometric stiffness and high tendon axial stiffness, respectively. Vertical motion is caused by the first order wave forces, while horizontal motion is due to the second order wave forces of low forcing frequency, [7].

Horizontal motion of TLP is nonlinear, since restoring stiffness is a function of surge, sway and yaw. Stiffness of vertical motion is almost linear and slightly depends on platform set-down caused by the offset as a position parameter. Value of set-down is limited in platform design, [8].

In dynamic analysis of TLPs, the secant stiffness matrix from [9], based on the equilibrium of restoring forces due to large displacements, is commonly used, [10, 11]. That formulation

results in larger values of surge, sway and yaw stiffness elements, since tendon axial stiffness of increased buoyancy is taken into account. That problem is analysed in details in [12].

The above shortcomings are overcome in [13]. The stiffness matrix is derived by the energy approach and application of Lagrange's equations. Dynamic analysis of TLP is performed by uncoupled and fully coupled models [14]. In the former case, the platform is considered as a rigid body without tendon influence. Fully coupled model is 3D FEM model of platform and tendons adapted to large displacements. Due to mechanical and hydrodynamic nonlinearity, the problem is solved in the time domain.

Since the uncoupled dynamic analysis of TLPs is mainly performed using linear stiffness matrix or inadequate nonlinear stiffness matrix, an effort for derivation of consistent stiffness matrix is undertaken in [15]. The force equilibrium approach is employed, and stiffness matrix similar to that in [13], determined by the energy approach, is derived with some additional coupling terms for surge, sway and yaw.

The relevant literature mainly deals with square TLPs. However, nowadays building of triangular TLPs as floaters for offshore wind turbines have become actualised. Therefore, in this paper, the nonlinear stiffness matrix for triangular TLP is presented. The same approach, i.e. the equilibrium of forces and the energy balance, as in [2] for square TLPs, is used. In order to evaluate two different restoring stiffness formulations, static response of a triangular TLP exposed to surge force and yaw moment are analysed. The obtained results are compared to those determined by FEM analysis.

2. STIFFNESS OF IN-PLANE MOTION BASED ON EQUILIBRIUM OF FORCES

2.1 LARGE DISPLACEMENTS

A triangular tension leg platform (TLP), with three tendons and main parameters is shown in Figure 1. The platform performs large motion consisting of surge, sway and yaw, δ_x, δ_y and φ, respectively, which are transmitted to all tendons, Figure 2. Trajectory of the tendon top, denoted as platform node due to yaw is a circular one, $r\varphi$, where r is the tendon radial distance from the platform centroid. The tendon offset is the secant displacement, Figure 2:

$$\delta_\varphi = 2r\sin\frac{\varphi}{2}. \tag{1}$$

According to Figure 2, the tendon top coordinates in an offset position can be expressed in the local coordinate system as:

$$L_{xn} = \delta_x - \Delta_{xn} = \delta_x - \delta_\varphi \sin\left(\vartheta_n + \frac{\varphi}{2}\right), \tag{2}$$

$$L_{yn} = \delta_y + \Delta_{yn} = \delta_y + \delta_\varphi \cos\left(\vartheta_n + \frac{\varphi}{2}\right), \tag{3}$$

$$L_{zn} = \sqrt{L^2 - L_{xn}^2 - L_{yn}^2} = L\sqrt{1 - g_1 + g_{2n}}, \tag{4}$$

$$g_1 = \frac{1}{L^2}\left(\delta_x^2 + \delta_y^2 + \delta_\varphi^2\right), \tag{5}$$

$$g_{2n} = \frac{2\delta_\varphi}{L^2}\left[\delta_x \sin\left(\vartheta_n + \frac{\varphi}{2}\right) - \delta_y \cos\left(\vartheta_n + \frac{\varphi}{2}\right)\right], \quad \textbf{(6)}$$

where L is the tendon length and ϑ_n, $n=1, 2, 3$, is the tendon central angle.

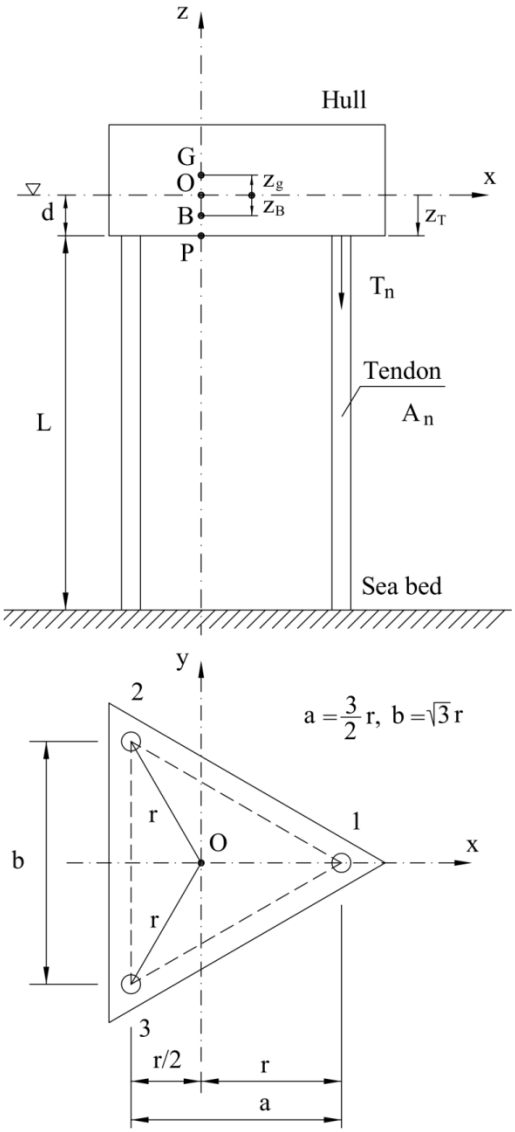

Fig. 1 *Triangular TLP*

Components of the tendon tension force in an offset position are proportional to the tendon top coordinates, i.e.

$$T_{xn} = \frac{T_n}{L}\left[\delta_x - \delta_\varphi \sin\left(\vartheta_n + \frac{\varphi}{2}\right)\right], \quad \textbf{(7)}$$

$$T_{yn} = \frac{T_n}{L}\left[\delta_y + \delta_\varphi \cos\left(\vartheta_n + \frac{\varphi}{2}\right)\right], \quad \textbf{(8)}$$

$$T_{zn} = \frac{T_n}{L} L_{zn}, \quad \textbf{(9)}$$

where T_n is the initial tendon tension force. Hence, the initial total platform force is $T = \sum_{n=1}^{N} T_n$.

Components of the platform force in an offset position, according to Eqs. (7), (8) and (9), read:

$$T_x = \sum_{n=1}^{N} T_{xn} = \frac{T}{L}\delta_x , \tag{10}$$

$$T_y = \sum_{n=1}^{N} T_{yn} = \frac{T}{L}\delta_y , \tag{11}$$

$$T_z = \sum_{n=1}^{N} T_{zn} = \frac{T}{N}\sum_{n=1}^{N} L_{zn} . \tag{12}$$

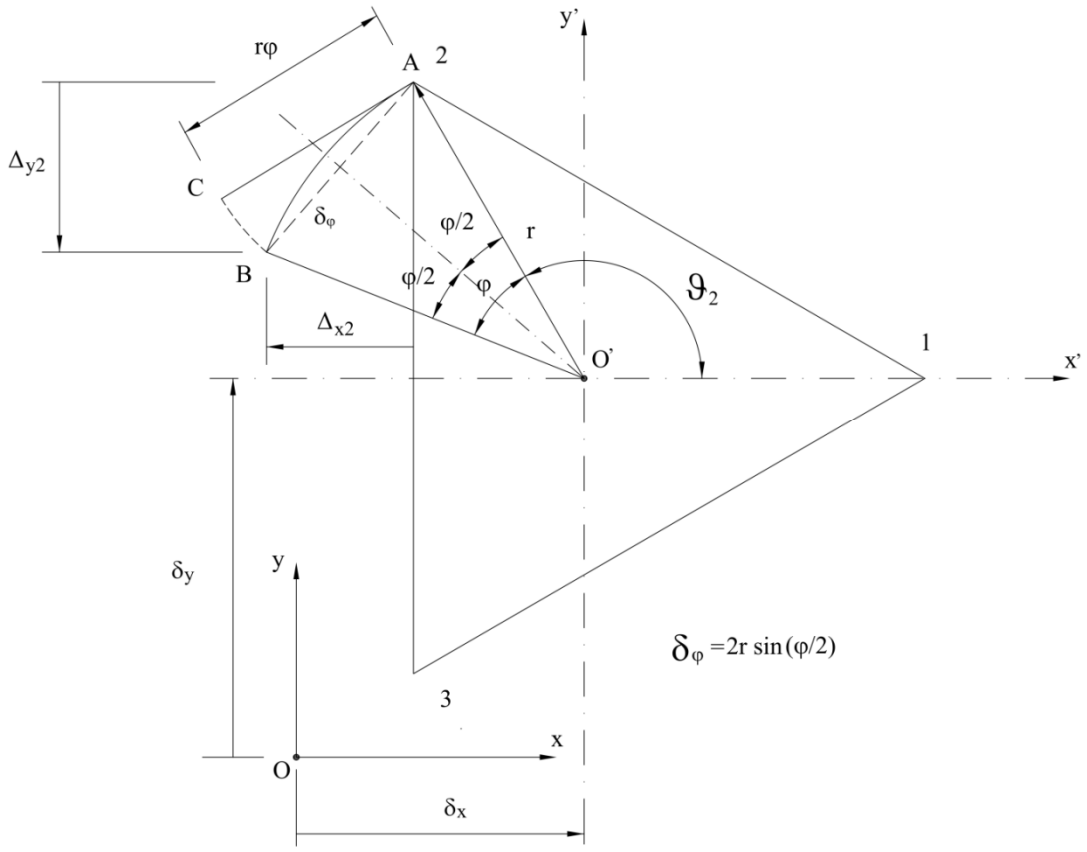

Fig. 2 *Large surge, sway and yaw,* δ_x, δ_y, δ_φ

Horizontal components T_x and T_y depend only on horizontal displacements δ_x and δ_y, since the trigonometric functions vanish from (7) and (8) upon summation of the given values of tendon central angle, ϑ_n, Table 1.

In order to make summation of L_{zn} in (12), it is necessary to expand function L_{zn} into the power series. Since $\sqrt{1-\varepsilon} = 1 - \frac{1}{2}\varepsilon - \frac{1\cdot 1}{2\cdot 4}\varepsilon^2 - \ldots$, the following is obtained:

$$L_{zn} = L\left(1 - \frac{1}{2}g_1 - \frac{1}{8}g_1^2\right) + L\left[\left(\frac{1}{2} + \frac{1}{4}g_1\right)g_{2n} - \frac{1}{8}g_{2n}^2\right]. \tag{13}$$

By taking into account Eqs. (7) and (8), as well as values of the trigonometric function from Table 1, one finds that $\frac{1}{N}\sum_{n=1}^{N} g_{2n} = 0$, while the tendon central angle ϑ_n vanishes from $\frac{1}{N}\sum_{n=1}^{N} g_{2n}^2$. As a result, the following is obtained:

$$L_z = \frac{1}{N}\sum_{n=1}^{N} L_{zn} = L\left(1 - f_1 - f_2\right), \tag{14}$$

where:

$$f_1 = \frac{1}{2L^2}\left(\delta_x^2 + \delta_y^2 + \delta_\varphi^2\right), \tag{15}$$

$$f_2 = \frac{1}{2} f_1^2 + f_3, \tag{16}$$

$$f_3 = \frac{\delta_\varphi^2}{4L^4}\left(\delta_x^2 + \delta_y^2\right). \tag{17}$$

Table 1 *TLP node parameters*

Node n	ϑ_n	$\widehat{\vartheta_n}$	$\sin\vartheta_n$	$\cos\vartheta_n$	x_n	y_n
1	*0*	*0*	*0*	*1*	r	*0*
2	*120°*	$\frac{2}{3}\pi$	$\frac{\sqrt{3}}{2}$	$-\frac{1}{2}$	$-\frac{1}{2}r$	$\frac{\sqrt{3}}{2}r$
3	*240°*	$\frac{4}{3}\pi$	$-\frac{\sqrt{3}}{2}$	$-\frac{1}{2}$	$-\frac{1}{2}r$	$-\frac{\sqrt{3}}{2}r$

The tendon offset causes platform set-down $\delta^S = L - L_z$, and additional buoyancy ΔU and tension forces ΔT_n. The total additional tendon force is determined from the equilibrium of the vertical forces:

$$U + \Delta U = Q + \frac{1}{L}\sum_{n=1}^{N}\left(T_n + \Delta T_n\right) L_{zn}, \tag{18}$$

where Q is the platform weight. The increased buoyancy is:

$$\Delta U = \rho g A_{WL} \delta^S, \tag{19}$$

where A_{WL} is the waterplane area. By taking the floating condition $T = U - Q$ into account and by substituting (19) into (18), the total additional tendon force is:

$$\Delta T = \frac{1}{L_z}\sum_{n=1}^{N} \Delta T_n L_{zn} = \frac{1}{L_z}\left(T + \rho g A_{WL}\right)\delta^S. \tag{20}$$

The horizontal components of the total tendon forces, Eq. (10), are increased and equalled to the external forces, $T_x = F_x$ and $T_y = F_y$, i.e.

$$F_x = \frac{1}{L}\left(T + \Delta T\right)\delta_x = \tilde{K}_{11}\delta_x,$$
$$F_y = \frac{1}{L}\left(T + \Delta T\right)\delta_y = \tilde{K}_{22}\delta_y, \tag{21}$$

where $\tilde{K}_{11}$ and $\tilde{K}_{22}$ represent surge and sway stiffness, respectively. Substituting (20) into (21), the following is yielded:

$$\tilde{K}_{11} = \tilde{K}_{22} = \tilde{K}_0 = \frac{1}{L_z}\left(T + \rho g A_{WL}\delta^S\right), \tag{22}$$

where $\tilde{K}_0$ is the nonlinear secant stiffness.

In order to determine yaw stiffness, let us specify the yaw moment due to action of the horizontal tendon forces, Figure 3:

$$M_z = -\sum_{n=1}^{N}\left(T_{xn} + \Delta T_{xn}\right)y_n + \sum_{n=1}^{N}\left(T_{yn} + \Delta T_{yn}\right)x_n, \tag{23}$$

where x_n and y_n are the tendon top coordinates, Table 1. By substituting Eqs. (7) and (8) into (23), the following is yielded:

$$M_z = \frac{1}{L}\sum_{n=1}^{N}\left(T_n + \Delta T_n\right)\left\{-\left[\delta_x - \delta_\varphi \sin\left(\vartheta_n + \frac{\varphi}{2}\right)\right]y_n + \right.$$
$$\left. + \left[\delta_x + \delta_\varphi \cos\left(\vartheta_n + \frac{\varphi}{2}\right)\right]x_n\right\}. \tag{24}$$

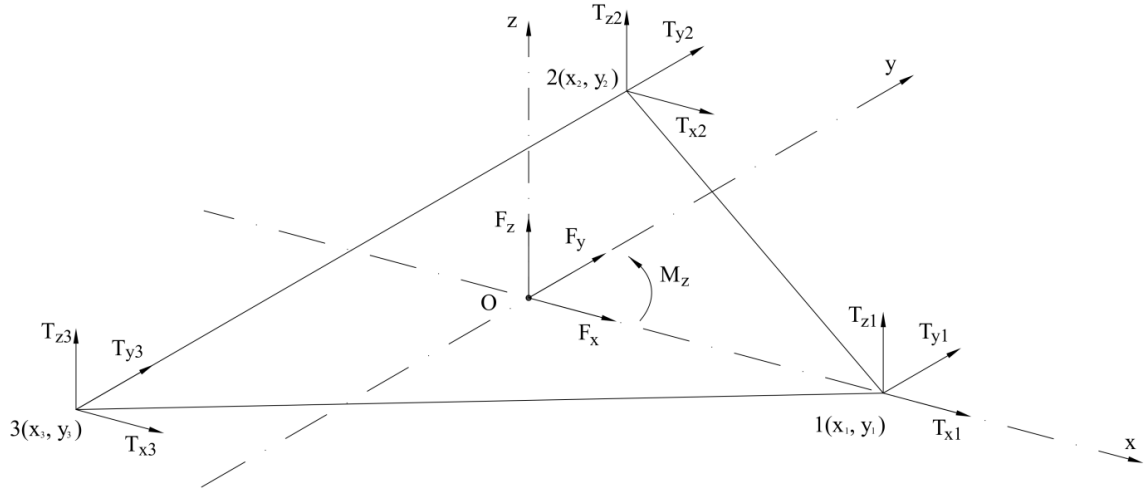

Fig. 3 *Tendon and platform forces*

Employing values of $\sin\vartheta_n$, $\cos\vartheta_n$, x_n and y_n from Table 1, the following is obtained upon summation:

$$M_z = \tilde{K}_0 r^2 \sin\varphi = \tilde{K}_{66}\varphi, \tag{25}$$

where $\tilde{K}_0$ is presented in Eq. (22). Finally, the yaw stiffness reads:

$$\tilde{K}_{66} = \tilde{K}_0 r^2 \frac{\sin\varphi}{\varphi}. \tag{26}$$

Value of the yaw stiffness is decreased from the maximum value at $\varphi = 0$, to the zero value at $\varphi = \pi/2$.

2.2 SMALL DISPLACEMENTS

If the platform displacements are small, the second order terms in (14) for L_z can be omitted, and for the set-down the following is obtained:

$$\delta^S = L - L_z = Lf_1 = \frac{1}{2L}\left(\delta_x^2 + \delta_y^2 + \delta_\varphi^2\right), \tag{27}$$

where $\delta_\varphi = r\varphi$, Eq. (1). In this case the set-down, as a result of platform offset, can be constructed in a simple way as shown in Figure 4. The yaw stiffness, Eq. (26), is also simplified, i.e. $\tilde{K}_{66} = \tilde{K}_0 r^2$. Hence, the restoring stiffness for all horizontal displacements depends on the common parameter $\tilde{K}_0$, Eq. (22).

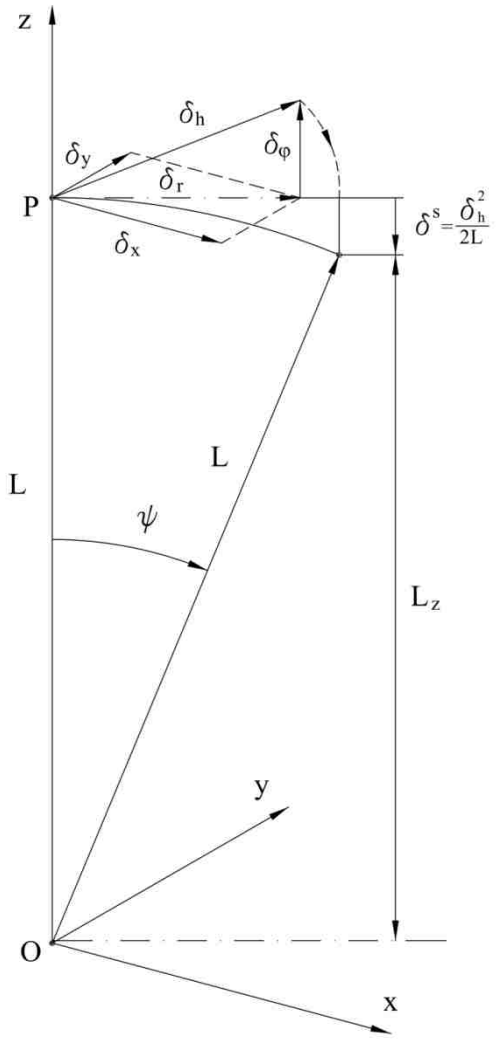

Fig. 4 *Construction of set-down in offset plane*

3. STIFFNESS OF IN-PLANE MOTION BASED ON BALANCE OF POTENTIAL ENERGY

3.1 LARGE DISPLACEMENTS

TLP is exposed to action of the following forces: Q, T, U, ΔT and ΔU. Tendon elongation ΔL_n due to tendon forces $T_n + \Delta L_n$ is quite small compared to the platform set-down, and therefore can be ignored. Work of the resulting external force, $T = U - Q$ is realised in the way of set-down, δ^S. The reacting internal force is buoyancy variation ΔU, Eq. (19), which is increased proportionally to the set-down. Hence, the platform potential energy can be presented in the form:

$$V = T\delta^S + \frac{1}{2}\rho g A_{WL}\left(\delta^S\right)^2. \tag{28}$$

The platform vertical coordinate L_z is defined by Eq. (14), and the set-down, $\delta^S = L - L_z$, takes the following form:

$$\delta^S = L\left(f_1 + f_2\right). \tag{29}$$

where functions f_1 and f_2 are defined by Eqs. (15) and (16).

On the other hand, L_z can be also determined as the quadratic mean of tendon vertical coordinates, Eq. (4), i.e.

$$L_z^2 = \frac{1}{N}\sum_{n=1}^{N}\left(L_{zn}\right)^2. \tag{30}$$

Since trigonometric functions of angles ϑ_n in L_{zn} vanish upon summation, Eq. (30) yields:

$$L_z^2 = L^2\left(1 - 2f_1\right). \tag{31}$$

Furthermore, relation $\delta^S = L - L_z$ gives:

$$\left(\delta^S\right)^2 = L^2 - 2LL_z + L_z^2. \tag{32}$$

and by substituting (14) and (31) into (32), the following is yielded:

$$\left(\delta^S\right)^2 = 2L^2 f_2. \tag{33}$$

Finally, substituting (29) and (33) into (28) results in:

$$V = TLf_1 + CLf_2, \tag{34}$$

where:

$$C = T + \rho g A_{WL} L. \tag{35}$$

Derivatives of potential energy per displacements represent restoring forces. Hence, for the secant stiffness of surge, sway and yaw, the following applies:

$$\tilde{K}_{11}^* = \frac{L}{\delta_x}\left(T\frac{\partial f_1}{\partial \delta_x} + C\frac{\partial f_2}{\partial \delta_x}\right), \tag{36}$$

$$\tilde{K}_{22}^{*}=\frac{L}{\delta_y}\left(T\frac{\partial f_1}{\partial \delta_y}+C\frac{\partial f_2}{\partial \delta_y}\right), \tag{37}$$

$$\tilde{K}_{66}^{*}=\frac{L}{\varphi}\left(T\frac{\partial f_1}{\partial \varphi}+C\frac{\partial f_2}{\partial \varphi}\right). \tag{38}$$

Derivatives of functions f_1 and f_2, Eqs. (15) and (16), are the following:

$$\frac{\partial f_1}{\partial \delta_x}=\frac{1}{L^2}\delta_x,\ \frac{\partial f_1}{\partial \delta_y}=\frac{1}{L^2}\delta_y,\ \frac{\partial f_1}{\partial \varphi}=\frac{r^2}{L^2}sin\varphi, \tag{39}$$

$$\frac{\partial f_2}{\partial \delta_x}=\frac{1}{L^2}f_1\delta_x+\frac{2r^2}{L^4}\delta_x sin^2\frac{\varphi}{2}, \tag{40}$$

$$\frac{\partial f_2}{\partial \delta_y}=\frac{1}{L^2}f_1\delta_y+\frac{2r^2}{L^4}\delta_y sin^2\frac{\varphi}{2}, \tag{41}$$

$$\frac{\partial f_2}{\partial \varphi}=\frac{r^2}{L^2}\left[f_1+\frac{1}{2L^2}\left(\delta_x^2+\delta_y^2\right)\right]sin\varphi. \tag{42}$$

By substituting Eqs. (39) – (42) into Eqs. (36), (37) and (38), the following is obtained:

$$\tilde{K}_{11}^{*}=\tilde{K}_{22}^{*}=\tilde{K}^{*}+2C\frac{r^2}{L^3}sin^2\frac{\varphi}{2}, \tag{43}$$

$$\tilde{K}_{66}^{*}=\left[\tilde{K}^{*}r^2+C\frac{r^2}{2L^3}\left(\delta_x^2+\delta_y^2\right)\right]\frac{sin\varphi}{\varphi}, \tag{44}$$

where:

$$\tilde{K}^{*}=\frac{1}{L}\left(T+C\frac{\delta^S}{L}\right), \tag{45}$$

and δ^S is presented by Eq. (29).

3.2 SMALL DISPLACEMENTS

If displacements are small:

$$\tilde{K}_{11}^{*}=\tilde{K}_{22}^{*}=\tilde{K}^{*}+C\frac{r^2}{L^3}\varphi^2, \tag{46}$$

$$\tilde{K}_{66}^{*}=\tilde{K}^{*}r^2+C\frac{r^2}{2L^3}\left(\delta_x^2+\delta_y^2\right), \tag{47}$$

and δ^S in $\tilde{K}^{*}$, Eq. (45), is presented by Eq. (27).

4. COMPARISON OF TWO IN-PLANE RESTORING STIFFNESS FORMULATIONS

Restoring stiffness for surge, sway and yaw, based on equilibrium of forces $\tilde{K}_{11}$, $\tilde{K}_{22}$ and $\tilde{K}_{66}$ are presented by Eqs. (22) and (26), while those based on energy balance, $\tilde{K}^*_{11}$, $\tilde{K}^*_{22}$ and $\tilde{K}^*_{66}$, by Eqs. (43) and (44). The latter includes some additional coupling terms. Also, there is a difference between the basic stiffness parameters $\tilde{K}_0$ and $\tilde{K}^*$, Eqs. (22) and (45). The following applies for said difference:

$$\tilde{K}^* - \tilde{K}_0 = \left(\frac{T}{L} - \rho g A_{WL} \right) \frac{\left(\delta^S \right)^2}{L L_z}, \tag{48}$$

which is of the second order of magnitude.

A numerical analysis of influence of different stiffness formulations on response of square TLP is performed in [15], Table 2.

Table 2 *Main particulars of TLP*

Parameter	*Symbol*	*Value*
Platform weight	Q	$3.3 \cdot 10^5$ kN
Buoyancy	U	$4.655 \cdot 10^5$ kN
Total tendon pre-tension	T	$1.355 \cdot 10^5$ kN
Column spacing	b	75.66 m
Column diameter	D	16.39 m
Tendon length	L	269 m
Water depth	$L+d$	300 m
Water plane area	A_{WL}	633 m²
Tendon cross-section area	A_n	0.05 m²
Young's modulus	E	$2.1 \cdot 10^8$ kN/m²
Tendon stiffness	EA_n/L	$3.4 \cdot 10^4$ kN/m
Hydrostatic stiffness	k_n	$2.07 \cdot 10^3$ kN/m
Centre of gravity above keel	$\overline{KG}$	27.47 m
Distance of columns from CG	$r = b/\sqrt{3}$	43.682 m

The following values of basic displacements for the considered triangular TLP are used: $\delta_x = 0.1L = 26.9$ m, $\varphi = 30° = 0.523598$ rad. The derived displacements read: approximate yaw, $\delta_\varphi = r\varphi = 22.782$ m, real yaw, Eq. (1), $\delta_\varphi = 22.612$ m, approximate set-down, Eq. (27), $\delta^S = 2.317$ m, real set-down, Eq. (29), $\delta^S = 2.309$ m. The surge and the yaw stiffness for the approximate and real displacements in the case of the force equilibrium and energy balance formulation are listed in Table 3. Variation of stiffness due to the approximate and real displacements is negligible. Some discrepancies are noticeable for the force equilibrium and energy balance stiffness formulation.

Table 3 *Nonlinear surge and yaw stiffness,* $\delta_x = 26.9\ m$, $\varphi = 30°$

Case	*Approach*	K_{11} *(kN/m)*	K_{66} *(kNm)*	δ^S *(m)*
1	*Force equilibrium, approximate set-down*	*562.05*	$1.0724 \cdot 10^6$	*2.317*
2	*Force equilibrium, real set-down*	*561.84*	$1.0237 \cdot 10^6$	*2.309*
3	*Energy balance, approximate set-down*	*585.91*	$1.1355 \cdot 10^6$	*2.317*
4	*Energy balance, real set-down*	*585.05*	$1.1351 \cdot 10^6$	*2.309*

In order to analyse which of the stiffness formulations is more reliable, the above nonlinear problem is solved by the finite element method employing LS DYNA software, [16]. A quite simple FEM model is constructed, as shown in Figure 5. The platform is modelled as a 1m thick plate and each tendon has four beam elements.

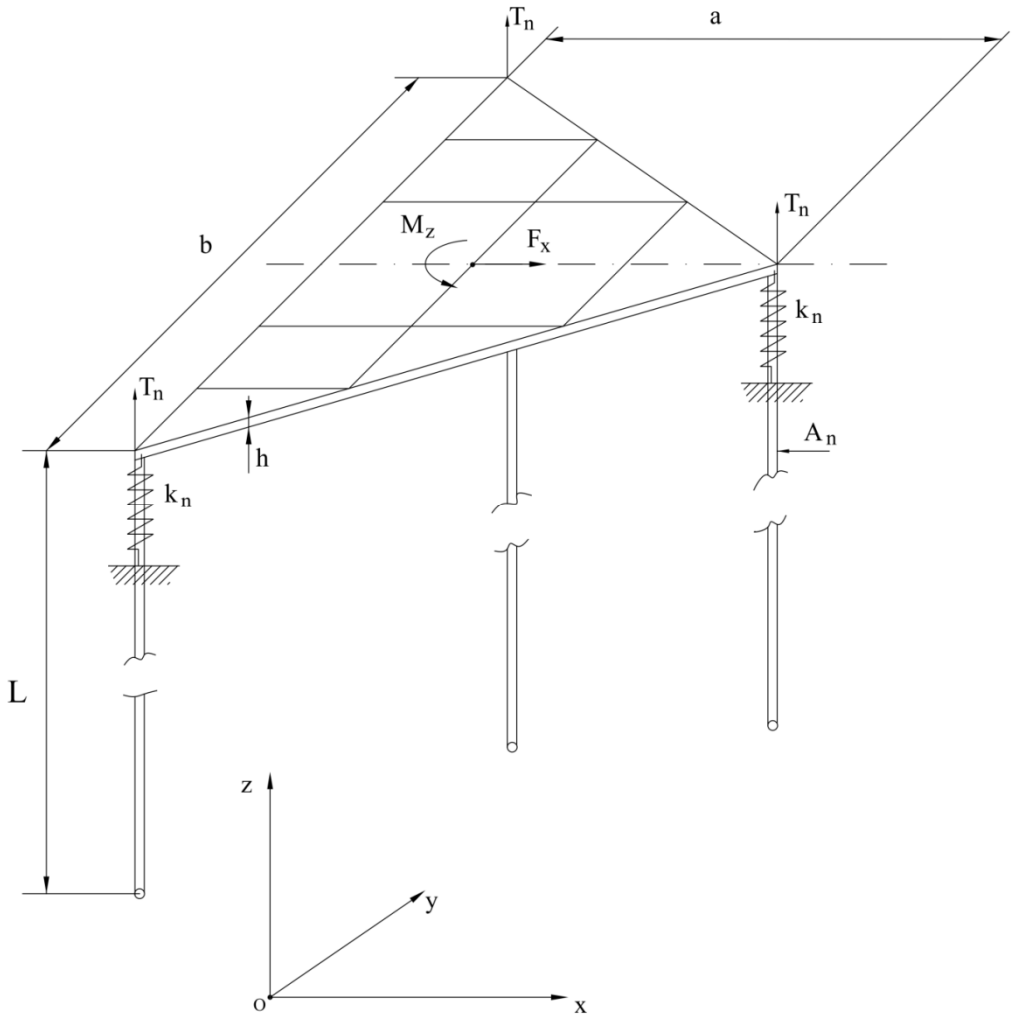

Fig. 5 *TLP FEM model*

The surge force and yaw moment are determined by the corresponding stiffness based on the force equilibrium (FE) and the energy balance formulation (EB), and the real displacements, Table 3: $F_{xFE} = \tilde{K}_{11}\delta_x = 1.511 \cdot 10^4$ kN, $M_{zFE} = \tilde{K}_{66}\varphi = 5.360 \cdot 10^5$ kNm, $F_{xEB} = \tilde{K}^*_{11}\delta_x = 1.574 \cdot 10^4$ kN, $M_{zEB} = \tilde{K}^*_{66}\varphi = 5.943 \cdot 10^5$ kNm. Force F_x is lumped in the plate corners, while moment M_z is distributed in all 16 nodes. The hydrostatic springs are placed in the plate corners with the equivalent stiffness of $k_n = \frac{1}{3}\rho g A_{WL} = 2070$ kN/m. Value of the Young's module is considerably increased ($E^* = 10^3 E$) in order to constrain the initial tendon strain due to the imposed tendon pretension force $T_n = T/3 = 4.517 \cdot 10^4$ kN, Figure 5.

A numerical calculation is performed separately for the particular loads F_x and M_z, and then for their simultaneous action. Static nonlinear problem of large displacements is solved by a general routine for dynamic problem in the time domain by the step-by-step explicit integration method and slowly increased load values in order to avoid influence of inertia. First force F_x is imposed and then moment M_z, so that their particular influence on the response can be noticed. The bird's view of the platform in the equilibrated translated and rotated position due to action of F_{zFE} and M_{zFE} is shown in Figure 6. Figures 7 and 8 represent the zoomed lateral and front view in which a small platform roll and pitch can be noticed.

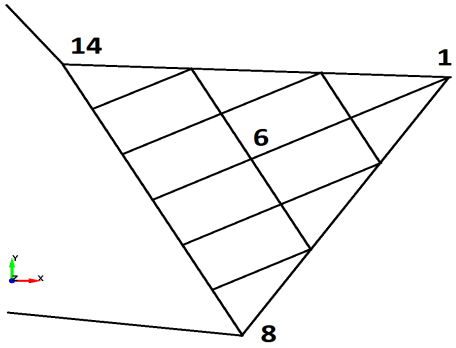

Fig. 6 *Bird's view of platform in offset position*

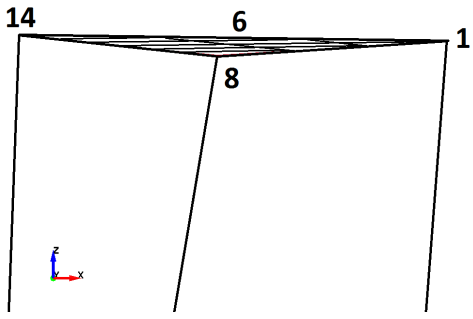

Fig. 7 *Lateral view of platform in offset position*

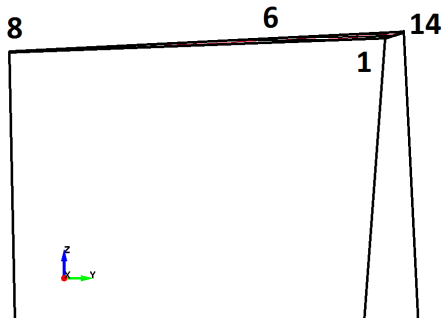

Fig. 8 *Front view of platform in offset position*

The time history of the platform longitudinal, transversal and vertical displacements is shown in Figures 9-11, respectively. During the F_{zFE} action the displacements of all three platform corners, as well as the centroid, are the same. Activation of M_{zFE} causes spreading of displacements due to the platform rotation. The displacements obtained using the FEM analysis based on the forced equilibrium approach (FE) and energy balance (EB) and the individual and simultaneous action of loads, F_x and M_z, are listed in Table 4. For F_x and M_z, FEM FE results are closer to the analytical input, whereas for the common action of F_x and M_z, FEM EB provides somewhat better results. Hence, both FE and EB restoring stiffness formulations are acceptable. However, since the real platform rotation is quite smaller than *30°*, a slight advantage for practical use can be given to the FE restoring stiffness formulation.

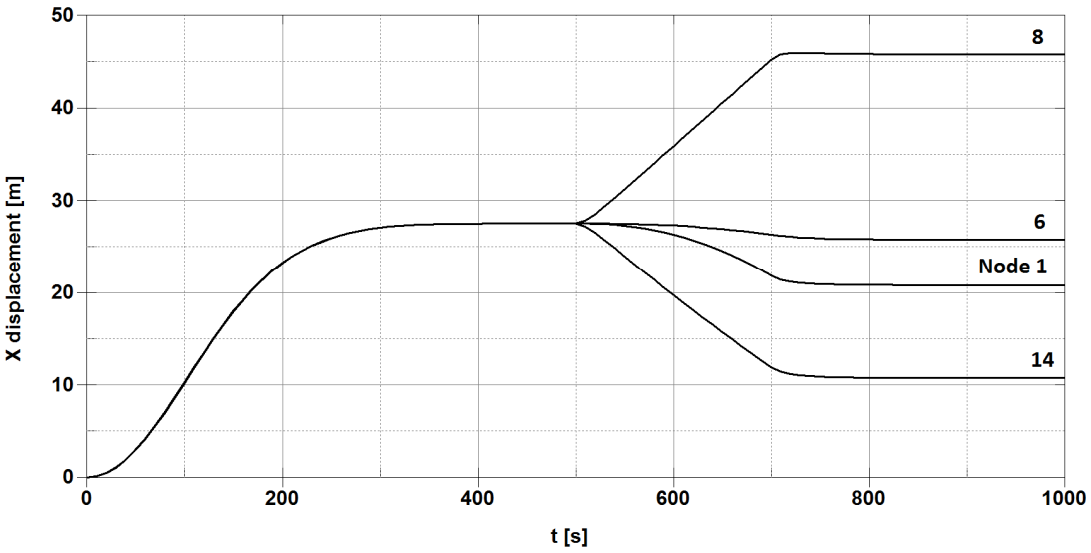

Fig. 9 *Time history of platform longitudinal displacement, Force Equilibrium (FE)*

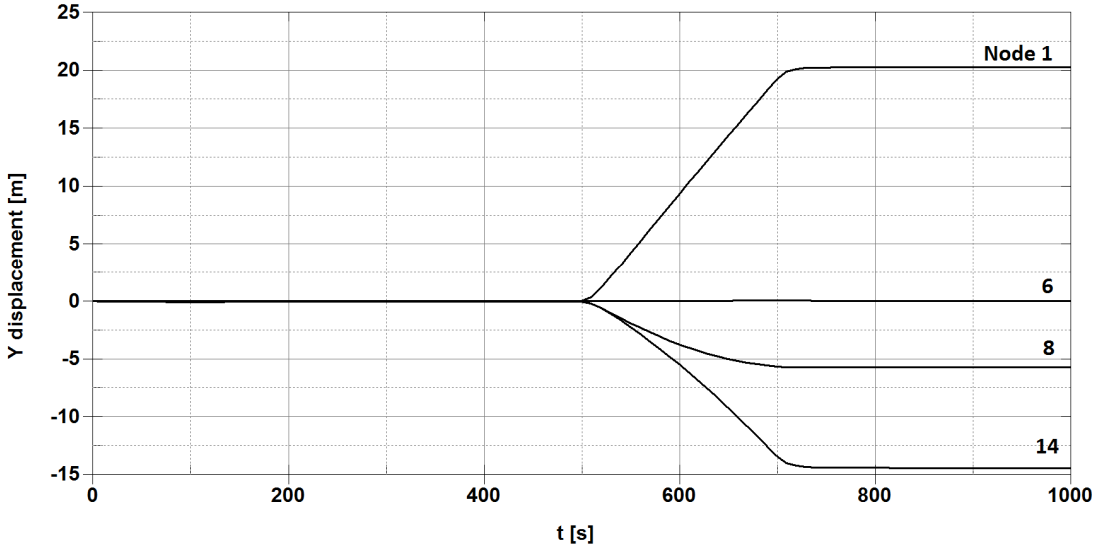

Fig. 10 *Time history of platform transverse displacement, Force Equilibrium (FE)*

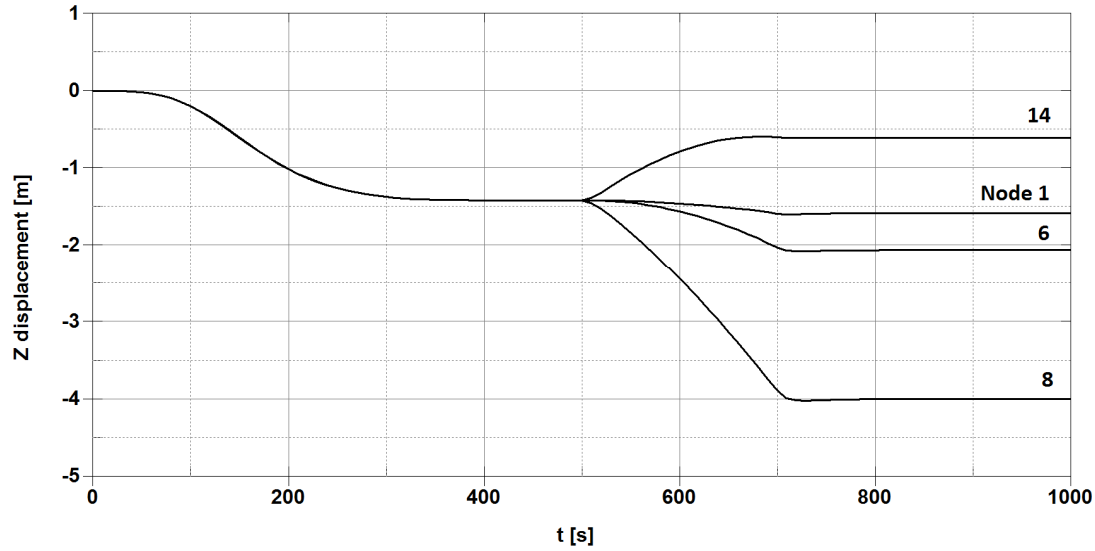

Fig. 11 *Time history of platform set-down, Force Equilibrium (FE)*

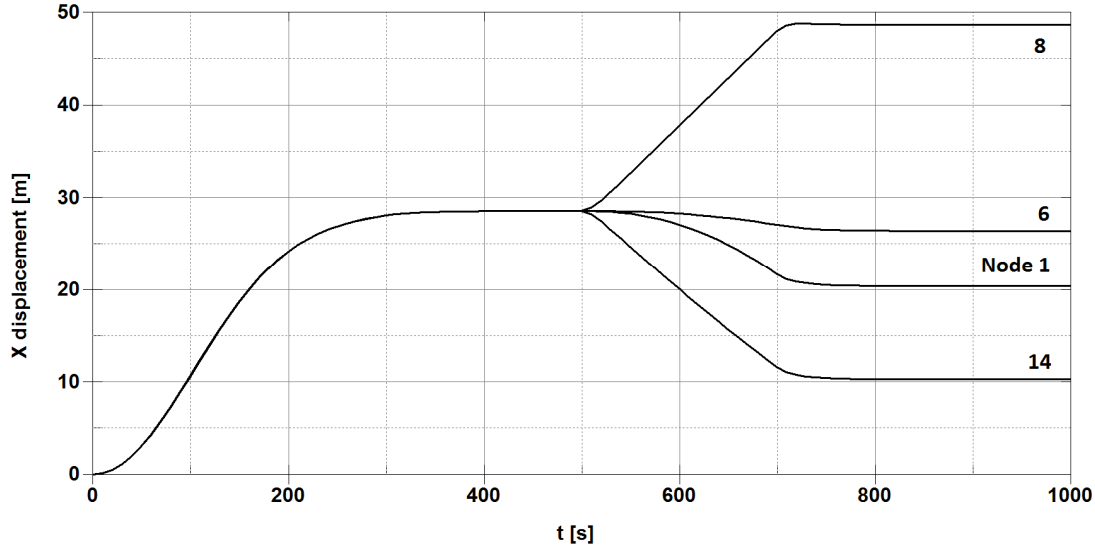

Fig. 12 *Time history of platform longitudinal displacement, Energy Balance (EB)*

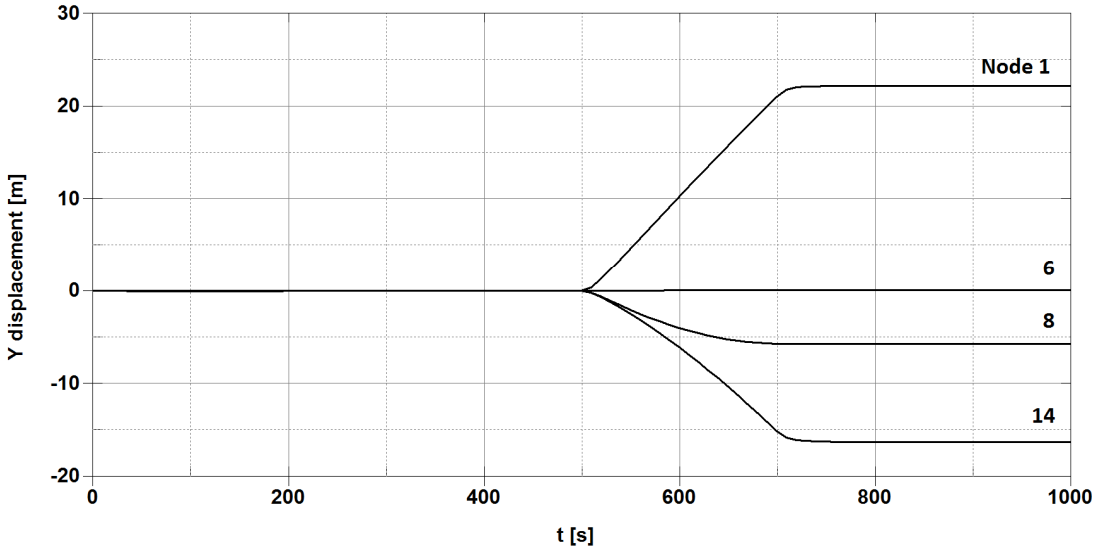

Fig. 13 *Time history of platform transfer displacement, Energy Balance (EB)*

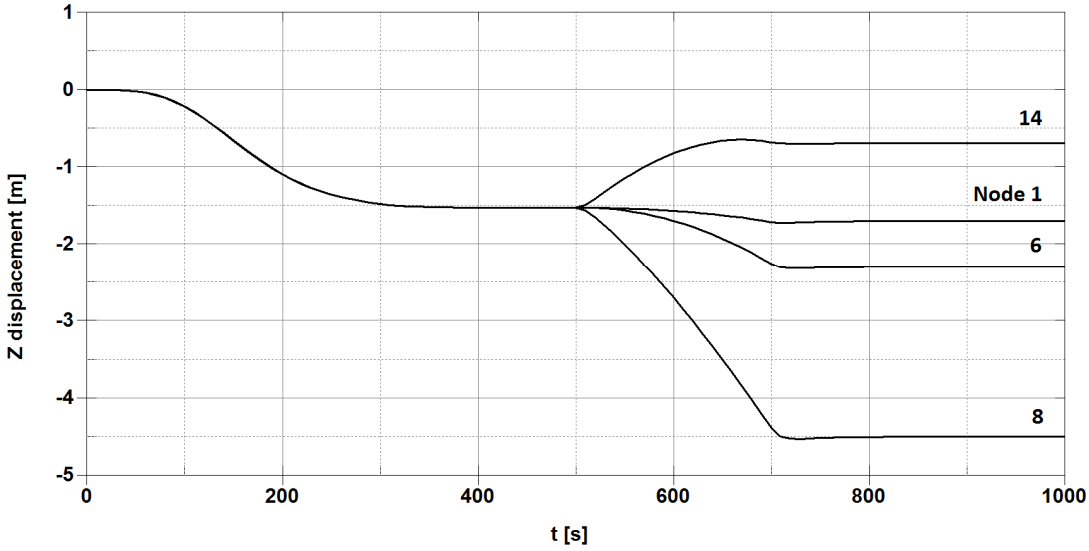

Fig. 14 *Time history of platform set-down, Energy Balance (EB)*

Table 4 *Platform displacements*

Case	*Approach*	F_x		M_z		F_x & M_z		
		δ_x (m)	δ^S (m)	φ	δ^S (m)	δ_x (m)	φ	δ^S (m)
1	*Analytical*	*26.900*	*1.348*	*30°*	*0.952*	*26.900*	*30°*	*2.309*
2	*FEM, FE*	*27.577*	*1.416*	*31°*	*1.006*	*25.835*	*27.5°*	*2.060*
3	*FEM, EB*	*28.602*	*1.524*	*34.5°*	*1.232*	*26.454*	*30.5°*	*2.296*

5. CONCLUSION

Dynamic behaviour of TLPs substantially depends on the nonlinear restoring stiffness. In dynamic analysis, the stiffness matrix derived in [10, 11] is ordinarily used. However, that formulation is not reliable enough, as explained in [13]. Therefore, a new formulation of the restoring stiffness matrix, based on both the equilibrium of forces and energy balance, is presented in [12]. A detailed analysis of the problem related to square TPLs, is undertaken and the obtained results are validated by the FEM analysis, [15].

In this paper, a similar analysis is performed for the derivation of the restoring stiffness for triangular TLPs. A correlation analysis of the analytical and numerical results shows that the restoring stiffness determined by both the force equilibrium and energy balance are reliable enough for a practical application.

DECLARATION REGARDING CONFLICT OF INTEREST

The authors declare that there is no conflict of interest.

FUNDING

This research received no specific grant from any funding agency in the public, commercial or non-profit sector.

6. REFERENCES

[1] S. Chakrabarti, Handbook of Offshore Engineering, Elsevier Science, 2005.

[2] Planning, designing and constructing tension leg platforms, API recommended practice 2T, 3rd ed., American Petroleum Institute, 2010.

[3] J. Veie and S.H. Holtberget, Three span floating suspension bridge crossing the Bjørnafjord, In: International Conference on Multi-Span Large Bridges, Porto, Portugal, pp. 373-380, 2015.

[4] J.J. Jensen and A.E. Mansour, Extreme motion predictions for deepwater TLP floaters for offshore wind turbines, In: Hydroelasticity in Marine Technology (Hydroelasticity 2006), Beijing, China, pp. 361-367, 2006.

[5] X. Meng, X. Liu, H. Tian, M. Liu and C. Wu, Optimal design and experimental evaluation of a TLP for FOWT at moderate water depth, In: Proceedings of the twenty-sixth International Ocean and Polar Engineering Conference (ISOPE), pp. 296-302, 2016.

[6] R. Adrezin, P. Bar-Avi and H. Benaroya, Dynamic response of compliant offshore structures-review, *J. Aerosp. Eng.*, Vol. 9, No. 4, pp. 114-31, 1996.

[7] O.M. Faltinsen and Z. Demirbilek, Hydrodynamic analysis of TLPs, In: Demirbilek Z, editor. Tension leg platform: state-of-the art review, ASCE, pp. 36-63, 1989.

[8] DNV-OS-C105 Structural design of TLP (LRF method). Det Norske Veritas, 2008.

[9] J. Morgan and D. Malaeb, Dynamic analysis of tension leg platforms, In: Proceedings of the second international offshore mechanics and arctic engineering symposium, pp. 31-37, 1983.

[10] A.K. Jain, Nonlinear coupled response of offshore tension leg platform to regular wave forces, *Ocean Eng.*, Vol. 24, No. 7, pp. 577-593, 1997.

[11] S. Chandrasekaran and A.K. Jain, Dynamic behaviour of square and triangular offshore tension leg platforms under regular wave load, *Ocean Eng.*, Vol. 29, No. 3, 279-313, 2002.

[12] I. Senjanović, M. Tomić and N. Hadžić, Formulation of consistent nonlinear restoring stiffness for dynamic analysis of tension leg platform and its influence on response, *Marine Struct.*, Vol. 30, No. 1, pp. 1-32, 2013.

[13] Y.M. Low, Frequency domain analysis of a tension leg platform with statistical linearization of the tendon restoring forces, *Marine Struct.*, Vol. 22, No. 3, pp. 480-503, 2009.

[14] J. Murray, C.K. Yang, W. Yang, P. Krishnaswamy and J. Zou, An extended tension leg platform design for Post-Katarina Gulf of Mexico, In: The proceedings of the nineteenth International Offshore and Polar Engineering Conference (ISOPE), Vol. 1, pp. 120-127, 2009.

[15] I. Senjanović, M. Tomić and S. Rudan, Investigation of nonlinear restoring stiffness in dynamic analysis of tension leg platform, *Engineering Struct.*, Vol. 56, pp. 117-25, 2013.

[16] LS DYNA theory manual, Livermore Software Technology Corporation, 2006.